Ion yields and erosion rates for Si1−xGex(0 ≤ x ≤ 1) ultralow energy O2+ secondary ion mass spectrometry in the energy range of 0.25–1 keV

R. J. H. Morris and M. G. Dowsett

Related Articles

Additional information on J. Appl. Phys.

Ion yields and erosion rates for Si$_{1-x}$Ge$_x$($0 \le x \le 1$) ultralow energy O$_2^+$ secondary ion mass spectrometry in the energy range of 0.25–1 keV

R. J. H. Morris[a] and M. G. Dowsett
Department of Physics, University of Warwick, Gibbet Hill Road, Coventry CV4 7AL, United Kingdom

We report the SIMS parameters required for the quantitative analysis of Si$_{1-x}$Ge$_x$ across the range of $0 \le x \le 1$ when using low energy O$_2^+$ primary ions at normal incidence. These include the silicon and germanium secondary ion yield [i.e., the measured ion signal (ions/s)] and erosion rate [i.e., the speed at which the material sputters (nm/min)] as a function of x. We show that the ratio R_x of erosion rates, Si$_{1-x}$Ge$_x$/Si, at a given x is almost independent of beam energy, implying that the properties of the altered layer are dominated by the interaction of oxygen with silicon. R_x shows an exponential dependence on x. Unsurprisingly, the silicon and germanium secondary ion yields are found to depart somewhat from proportionality to $(1-x)$ and x, respectively, although an approximate linear relationship could be used for quantification across around 30% of the range of x (i.e., a reference material containing Ge fraction x would give reasonably accurate quantification across the range of $\pm 0.15x$). Direct comparison of the useful (ion) yields [i.e., the ratio of ion yield to the total number of atoms sputtered for a particular species (ions/atom)] and the sputter yields [i.e., the total number of atoms sputtered per incident primary ion (atoms/ions)] reveals a moderate matrix effect where the former decrease monotonically with increasing x except at the lowest beam energy investigated (250 eV). Here, the useful yield of Ge is found to be invariant with x. At 250 eV, the germanium ion and sputter yields are proportional to x for all x. © *2009 American Institute of Physics*. [DOI: 10.1063/1.3139279]

I. INTRODUCTION

Silicon and germanium wafers have been used since the 1950s for semiconductor devices and their combination (Si$_{1-x}$Ge$_x$ for $0 \le x \le 1$) has been under investigation for high-mobility applications for around the last 20 yr. The benefits offered by SiGe for device performance have been realized through the production of highly planar, lattice mismatched epitaxial layers[1,2] with thicknesses in the nanometer range. Tailoring of the Ge fraction x controls the lattice mismatch, and thereby the tetragonal distortion in a strained epitaxial layer. In turn, this allows the band structure of the material to be engineered to suit a particular application.[3] Until recently, x-values of up to 0.4 were used in device fabrication. The novel devices planned for the future[4] will demand the whole range of x from 0 to 1. To obtain accurate quantitative analysis using ultralow energy secondary ion mass spectrometry (uleSIMS), the sputter and ion yields need to be established, and the dependence of depth resolution limiting effects such as the development of surface topography need to be investigated as a function of bombardment conditions.

Previous SIMS SiGe studies have been carried out predominantly using either oxygen or caesium primary ion bombardment at relatively high beam energies (≥ 2 keV) and for Si$_{1-x}$Ge$_x$ layers with $x \le 0.5$.[5,6] Recently there have been a few studies where lower bombardment energies (≥ 500 eV) and/or higher Ge levels have been examined.[7,8] The overall information obtained thus far however, is still somewhat limited. A major requirement is to determine the Ge profile at matrix levels in thin layers, especially after treatments such as annealing.

Here we seek to find conditions (if any) under which uleSIMS using O$_2^+$ ions can obtain accurate Ge profiles across the full concentration range, without distortion from matrix effects and variations in erosion rate. The incident beam energies used were in the range of 0.25–1 keV because the high depth resolution offered is essential for the study of layers on the nm thickness scale. We establish how both the silicon and germanium secondary ion yields vary with matrix content and beam energy, and quantify the erosion rate as a function of energy and composition. The measured silicon and germanium ion yields for different primary beam energies were compared to ascertain whether they were influenced by sputter yield alone (i.e., the ratio is constant), or a combination of sputter yield and ionization probability.

II. EXPERIMENTAL

The Si$_{1-x}$Ge$_x$ ($0 < x < 1$) wafers used for this work were grown using low energy dc-plasma enhanced chemical vapor deposition (LEPECVD) at EHT Zürich.[9] Eight wafers were produced using this growth method with nominal germanium percentages ranging from 15%–100% (see Table I for a listing of the actual intended values). The full structures consisted of a standard silicon substrate with a constant composition SiGe layer epitaxially deposited on top. The SiGe layer thicknesses for the individual wafers varied between 2.86–6.72 μm (refer to Table I for the individual sample thicknesses). As the wafer layer thicknesses exceeded the mechanical equilibrium thickness for strained SiGe layer

a)Electronic mail: r.morris@warwick.ac.uk.

TABLE I. Wafer identification, intended layer composition, intended layer thickness, and HRXRD measured composition of all the wafers used for this work.

Sample ID	Intended Ge fraction (%)	Relaxed lattice parameter (Å)	Measured HRXRD germanium content (%)	Layer relaxation (%)	Layer thickness (μm)
1	0	5.431	0	100	500
2	15	5.466	17	99.5	6.72
3	27	5.489	28	96.0	5.46
4	35	5.511	37	94.3	6.02
5	42	5.527	44	96.1	6.65
6	50	5.538	50	99.1	5.98
7	59	5.563	60	99.6	5.22
8	74	5.575	75	99.3	4.22
9	100	5.654	99	99.7	2.86
10	100	5.658	100	100	300

growth,[10] all of the samples were expected to be fully relaxed. We have shown that low energy SIMS measurements of strained and relaxed $Si_{1-x}Ge_x$ layers ($x \leq 0.3$) (Ref. [7]) yield near identical results and there is no reason to believe this transferability will change for the extended range of ($0 < x < 1$). The similarity in erosion rate behavior as a function of x (for all beam energies) indicates that the altered layer stoichiometry and its state is energy independent. Aside from the eight LEPECVD wafers, a (100) float zone silicon wafer and a (100) undoped germanium wafer were obtained, completing the set of samples used for this work.

The SIMS depth profiling was carried out using our Atomika 4500 quadrupole SIMS instrument. The primary beam energies used were 250 eV, 500 eV, 750 eV, and 1 keV with a constant beam current (± 0.2 nA) for each energy used. Normal incidence was used for all the measurements to reduce the likelihood of ripple formation. The primary beam was scanned over the same area for all the profiles measured; approximately 220×220 μm^2. The depths of the SIMS craters were measured using a Sloan Dektak 3030 stylus profilometer.

High resolution x-ray diffraction (HRXRD) was used to calibrate the germanium concentration levels of all of the LEPECVD layers [Philips HRXRD diffractometer system using Cu $K\alpha_1$ x rays (wavelength of 0.154 nm)]. In order to determine the amount of germanium present within the individual layers, the bulk layer lattice parameter was determined from

$$a_{SiGe} = \left[\frac{(1-v)}{1+v} \right] a_{SiGe}^{\perp} + \left[\frac{2v}{(1+v)} \right] a_{SiGe}^{\parallel}, \qquad (1)$$

where v is Poisson's ratio;[11] $a^{\perp}$ and $a^{\parallel}$ are the out-of-plane and in-plane lattice parameters, respectively.

The in-plane and out-of-plane lattice parameters were determined experimentally through a combination of symmetric and asymmetric ω-2θ scans. Two symmetric scans taken about the (004) plane direction were used to determine the perpendicular (out-of-plane) lattice parameter ($a^{\perp}$), while two asymmetric scans were performed to determine the in-

plane lattice parameter ($a^{\parallel}$); one asymmetric scan used the (224) plane direction while the other used the ($\overline{2}\overline{2}4$) plane direction. From these scans the perpendicular lattice parameter was found by using

$$a_{SiGe}^{\perp} = \frac{2\lambda}{\sin(\theta_{004}^{Si} + \Delta\omega_{004})}, \qquad (2)$$

where θ_{004}^{Si} is the silicon substrate Bragg angle and $\Delta\omega_{004}$ the mean angular spacing between the silicon substrate peak and the constant composition SiGe layer peak. The in-plane lattice parameter ($a^{\parallel}$) was found from

$$a_{SiGe}^{\parallel} = \frac{\sqrt{2}\lambda}{\sqrt{(a_{SiGe}^{\perp})^2\sin^2(\theta_{224}^{Si} + \Delta\omega_{224} - 4\lambda^2)}} a_{SiGe}^{\perp}, \qquad (3)$$

where θ_{224}^{Si} is the (224) directional Bragg angle of the silicon substrate and $\Delta\omega_{224}$ the mean angular separation between the silicon and SiGe peaks for the respective (224) and ($\overline{2}\overline{2}4$) scans. Effects due to tilt present in the (224) planes with respect to the silicon substrate were compensated for by using the mean peak separation value combined with the 180° rotation about the surface normal between each of the symmetric and asymmetric scans.[12] Once the bulk lattice parameter was known the germanium content within the layer was obtained from the relationship[13]

$$a_{Si_{1-x}Ge_x} = xa_{Ge} + (1-x)a_{Si} - 0.00436x^3 + 0.03265x^2 - 0.02828x, \qquad (4)$$

where a_{Si} and a_{Ge} are the silicon and germanium lattice parameters, respectively; x is the mole fraction; and a_{SiGe} is the bulk SiGe lattice parameter.

III. RESULTS AND DISCUSSION

A. High resolution x-ray analysis

Figures 1(a) and 1(b) show the symmetric and asymmetric rocking curves obtained from the $Si_{0.65}Ge_{0.35}$ sample measured and are representative of those observed from all the layers analyzed by HRXRD; apart from the peak splitting distances and signal intensities, which vary for differing germanium composition. The HRXRD results are summarized in Table I and are in good agreement with the intended values. The accuracy of this measurement was believed to be ± 1 at. %. It was also established from the bulk lattice parameters that all the layers were fully relaxed (e.g., $>99\%$) as expected.

B. Secondary ion yield behavior of SiGe

Figures 2(a) and 2(b) show the silicon ($^{30}Si^+$) and germanium ($^{70}Ge^+$) secondary ion yields measured at 250 eV, respectively, and are representative of what was observed for all the energies used. The silicon ion yields (i.e., the secondary Si ions (ions/s)) show constant signals as a function of time (corresponding to depth); a good indication that the layers were of uniform composition, as intended. The silicon ion yields also behave as expected with germanium fraction: the higher the germanium level, the lower the silicon ion yield. In the case of the germanium ion yields, the 250 and
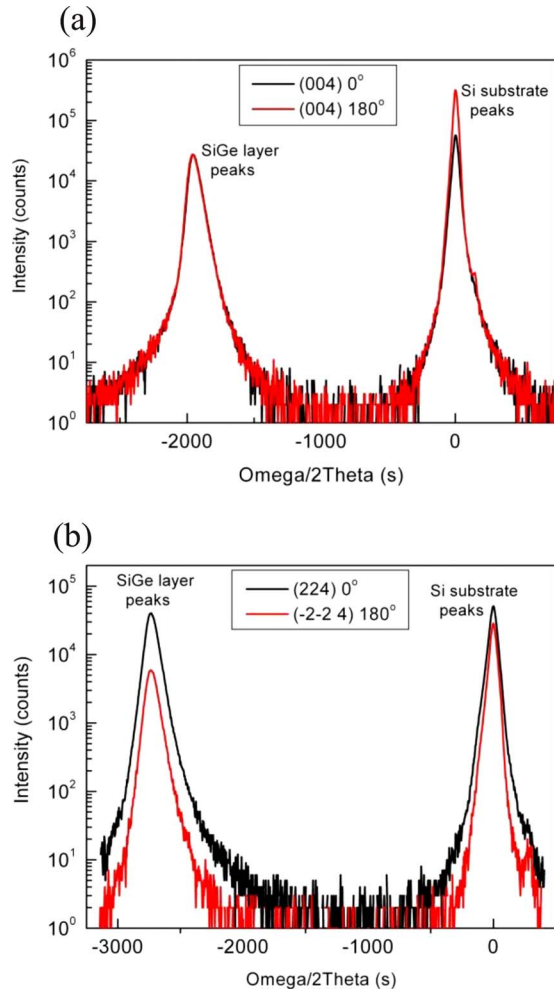
FIG. 1. (Color online) Measured HRXRD rocking curves of sample 4 (Si$_{0.65}$Ge$_{0.35}$). (a) Symmetrical HRXRD rocking curves. (b) Asymmetrical HRXRD rocking curves.
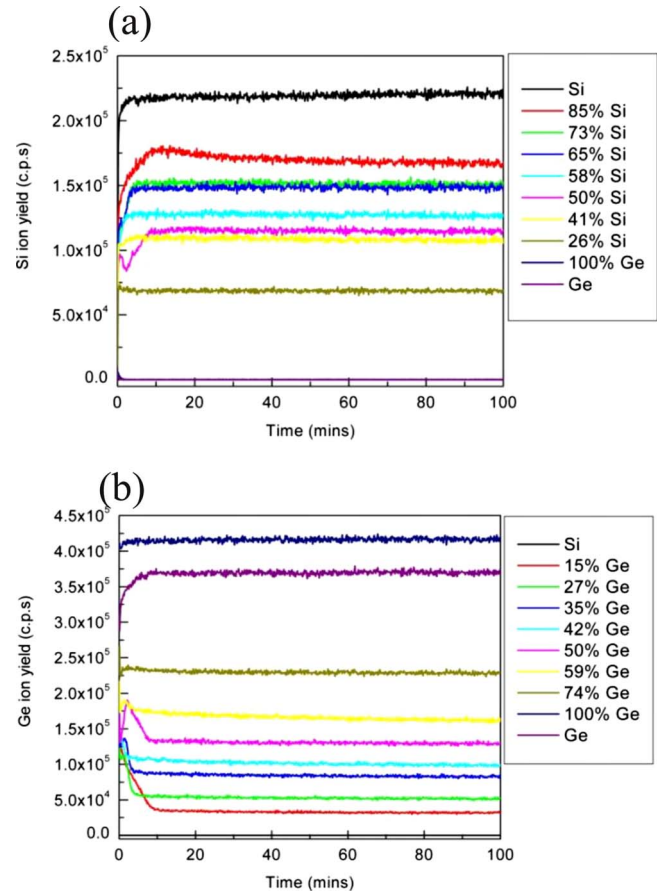

FIG. 2. (Color online) Measured (250 eV) ion yields from the silicon, SiGe, and germanium samples. (a) Silicon ion yields and (b) germanium ion yields.

500 eV showed a similar behavior to those seen for the silicon ion yields (i.e., constant secondary germanium ion yields as a function of time), and in this case the germanium ion yield increased with the germanium content. However, for the 100% LEPECVD and germanium substrate layers profiled at beam energies ≥750 eV, the germanium ion yield intensities were observed to drop as a function of depth or have a lower yield than those measured from certain SiGe layers [Fig. 3(a)]. This behavior is still under investigation although it appears to be related to the altered layer[14] and the development of large pits as discussed later in this paper.

The silicon ion yield from the "100%" germanium epilayer was a factor of 60 higher than that from the pure germanium substrate [Fig. 3(b)]. This indicates that there was a small amount of silicon present within the epilayer, a result which is in good agreement with that predicted by the x-ray analysis. There have been suggestions before that epitaxial growth systems have memory effects which can lead to the inadvertent incorporation of previously used elements.[15] This small silicon presence has other implications for the behavior of the material under oxygen bombardment and we discuss these later.

C. Erosion rate

Knowledge of the erosion rate is essential if quantitative SIMS analysis of any material is to be achieved, and this will, in general, vary with the alloy composition in SiGe.[16] All the wafers were profiled to produce craters well in excess of 100 nm in depth to ensure accurate measurement and relative insensitivity to any transient behavior.[17] The width of the transient region is highly dependent on both the beam energy and the material itself. Typically, it is found that the higher the beam energy the greater the transient width[18] and although the material dependence of this width is unknown for SiGe, we expect it to be in the range of 1–5 nm for the energies used here. The Dektak was calibrated immediately before the measurements to reduce any errors in the depth scale, and each crater was measured several (at least 3 times) times in different places and in two orthogonal directions. The average of the scans was then taken to be the crater depth, with the variation about the mean found to be less than ±2%.

Erosion rates were calculated by dividing the crater depth by the profile time. All the crater bottoms were smooth (at least to the surface profilometer) except for the ≥750 eV profile in pure germanium, where macroscopic roughening and pitting of the crater bottom was observed. Figures 4(a)–4(d) show typical crater profiles for these beam energies. The germanium epilayer shows only a small amount of
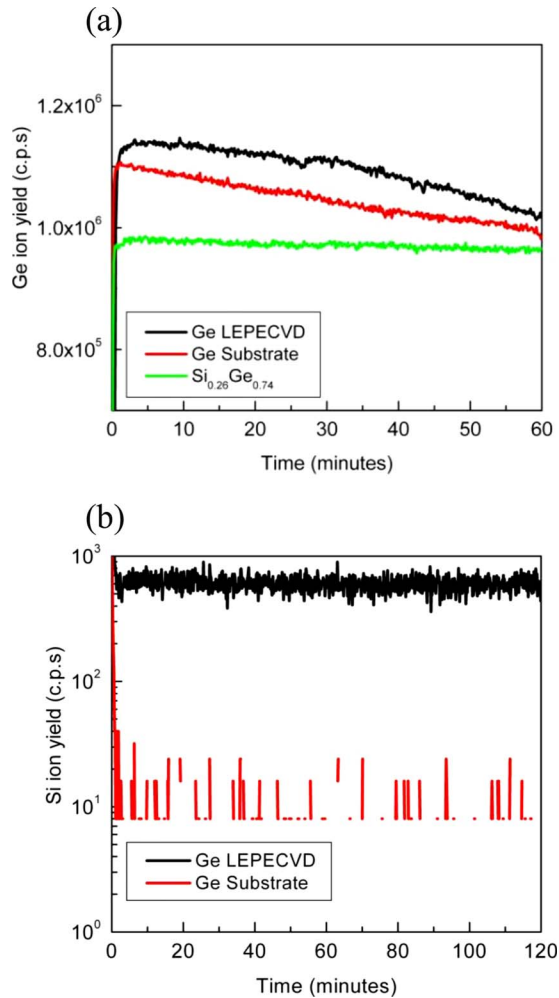
FIG. 3. (Color online) (a) Measured germanium ion yield (750 eV) from the LEPECVD germanium, germanium substrate, and the $Si_{0.26}Ge_{0.24}$ layer. (b) Measured silicon ion yields (1 keV) from the LEPECVD germanium layer and germanium substrate.
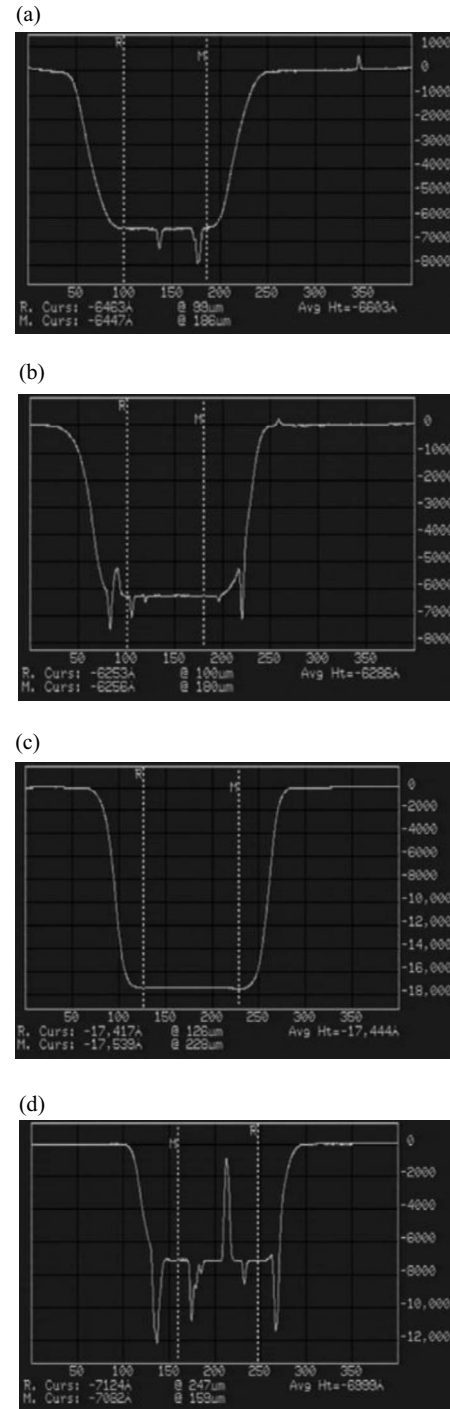
FIG. 4. Dektak images showing the craters for: (a) 750 eV 100% LEPECVD germanium layer, (b) 750 eV germanium substrate, (c) 1 keV 100% LEPECVD germanium layer, and (d) 1 keV Ge substrate.

roughening at 750 eV, while none is observed at 1 keV in this case. This is not a reproducible result and the layer does roughen in some 1 keV profiles. Figures 5(a) and 5(b) are optical and scanning electron microscopy (SEM) images of a typical crater produced on the germanium epilayer at 750 eV showing the beam induced topography. Pitting/roughening is not observed in these samples at energies ≤500 eV when measured using the surface profilometer and this was verified using both optical and SEM imaging, examples of which are given in Fig. 5(c). It was impossible to determine the depths of most of the high energy craters into pure germanium accurately but for the 750 eV profile of the epilayer there were regions between the pitting which were sufficiently flat for this purpose. These results are included for comparison.

The erosion rates measured for the SiGe and germanium were normalized to those found for silicon measured at the same primary beam energy. All the results are summarized in Table II, while Fig. 6(a) shows a plot of the normalized rates as a function of x. The behavior is independent of beam energy for the SiGe layers but not for pure germanium. (i.e., in the SiGe case the energy dependence of erosion rate is the same for both Si and SiGe so it disappears in the normaliza-

tion). From the silicon and SiGe normalized erosion rates [Fig. 6(b)], the variation R as a function of x is found to follow an expression of the form

$$R = A + B \exp(x/C), \tag{5}$$

where A, B, and C are constants with values of 0.77, 0.23, and 48.10, respectively.

The erosion rate of any material is dictated by the beam and material interaction, and so when a constant erosion rate (for a particular matrix) is obtained, this implies a constant
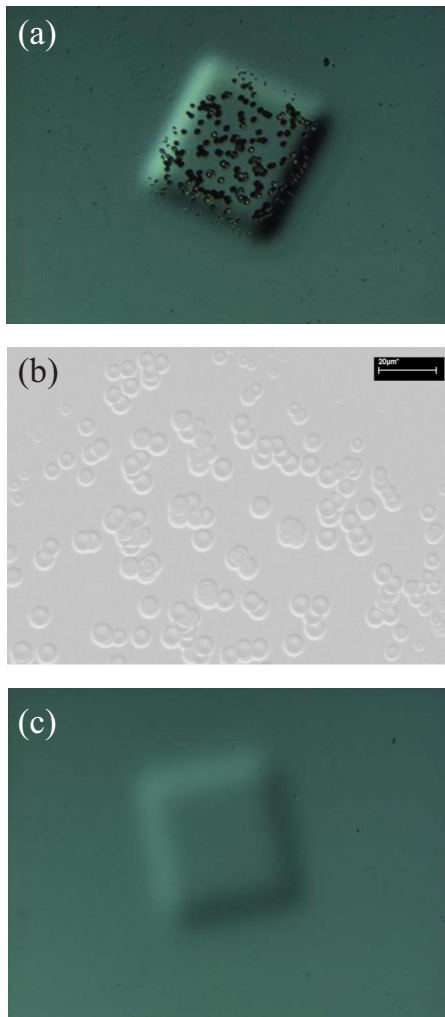
FIG. 5. (Color online) (a) Optical image of the LEPECVD germanium layer showing the large scale topography produced inside the crater by the 750 eV primary beam. (b) 10 keV SEM image of the same crater showing the induced topography change to be pits. (c) An optical image of a 250 eV crater in the LEPECVD germanium showing no topography change.

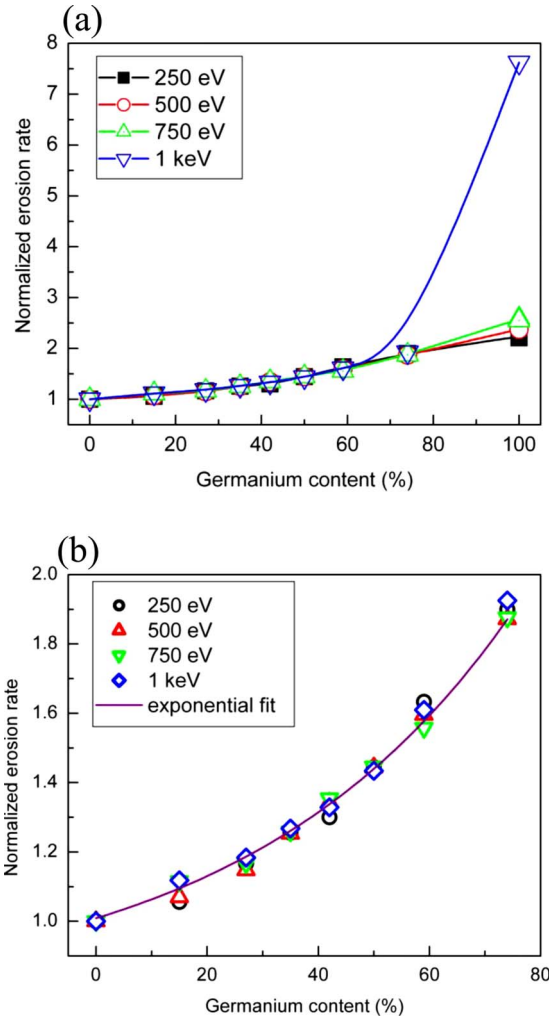FIG. 6. (Color online) (a) Normalized erosion rates as a function of germanium content for different primary beam energies. (b) Normalized silicon $Si_{1-x}Ge_x$ erosion rates and exponential fit as a function of germanium content.

near-surface composition has been established. In this case (i.e., SiGe); $1-x$ atoms of silicon are sputtered for every x atoms of germanium. It is well known that silicon preferentially oxidizes[14] and so it is very likely that the migration rate

TABLE II. Normalized erosion rates for the 250 eV, 500 eV, 750 eV, and 1 keV SIMS profiles of the various Si, $Si_{1-x}Ge_x$, and Ge layers.

Sample ID	Intended Ge fraction (%)	250 eV normalized erosion rate	500 eV normalized erosion rate	750 eV normalized erosion rate	1 keV normalized erosion rate
1	0	1.00	1.00	1.00	1.00
2	15	1.06	1.07	1.12	1.12
3	27	1.17	1.15	1.17	1.18
4	35	1.26	1.25	1.26	1.26
5	42	1.30	1.34	1.35	1.33
6	50	1.44	1.44	1.45	1.43
7	59	1.63	1.59	1.55	1.61
8	74	1.90	1.87	1.88	1.92
9	100	2.24	2.38	2.58	7.62
10	100	2.20	2.37	2.54	…

of silicon atoms into the altered layer (balanced by the sputtering of silicon from the surface at the same rate) controls the overall erosion rate (and consequently the steady state thickness of the altered layer).

Potentially, the normalized erosion rate could, because of its independence of beam energy, be used to determine the Ge fraction, or to confirm results from the ion yield. The accuracy and usefulness of this approach merits further investigation.

For pure germanium, the normalized erosion rate is dependent on primary beam energy [Fig. 6(a)]. Here a small difference exists between the normalized erosion rates of the 250, 500, and 750 eV conditions. A significant increase (approximately 3 fold) in the normalized erosion rate is observed between 750 eV and 1 keV.

D. Ion yield behavior

It has been previously shown that accurate SIMS matrix quantification for $Si_{1-x}Ge_x$ layers within the range of $x \leq 0.3$ can be achieved by taking the ratio of the silicon ion yield from the SiGe layer to that of pure silicon.[7,19] To test
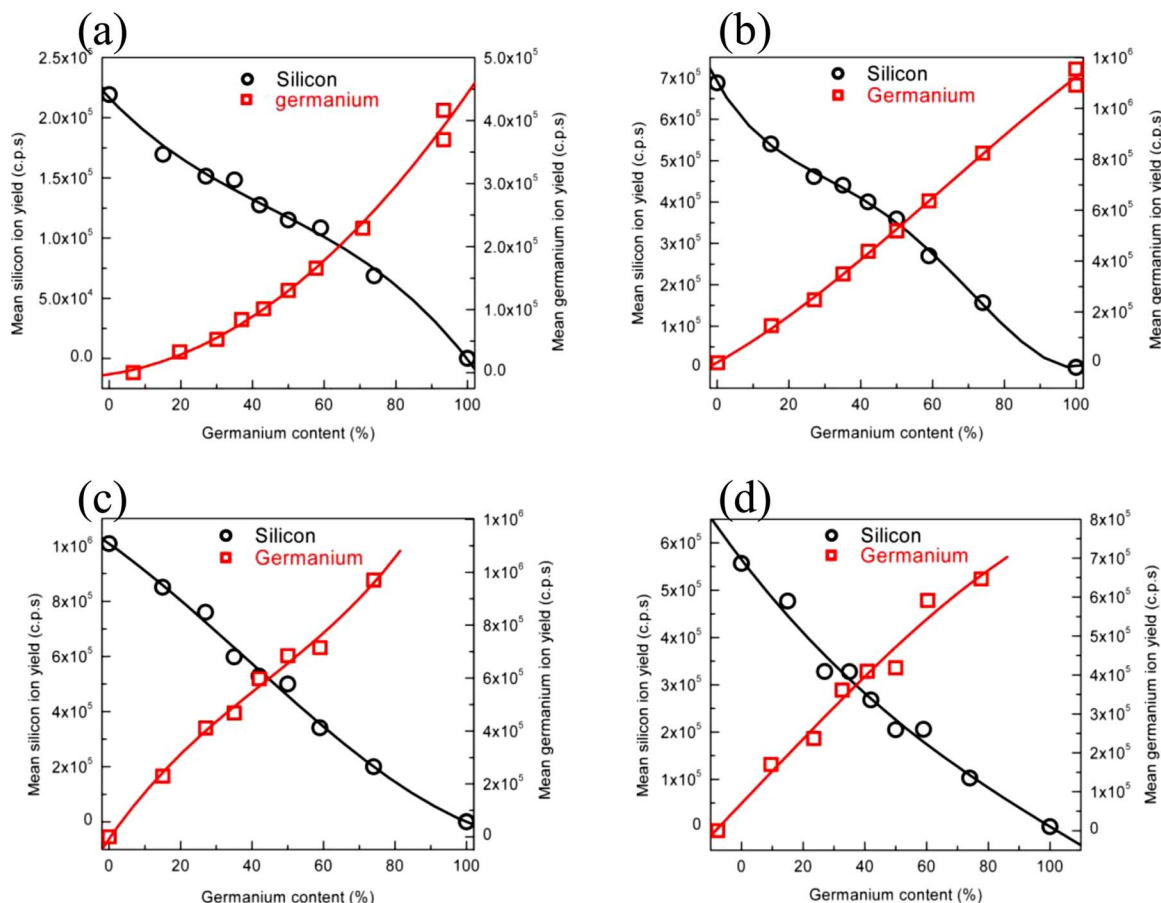
FIG. 7. (Color online) Mean silicon and germanium ion yields as a function of germanium content. (a) 250 eV, (b) 500 eV, (c) 750 eV, and (d) 1 keV.

this relationship over a larger range of x, the variation of the individual ion yields with matrix content using different primary beam energies was measured. Mean silicon and germanium ion yields were determined from the flat regions of the profiles shown in Figs. 2(a) and 2(b), avoiding the transient behavior. Figures 7(a)–7(d) show these as a function of x for the four primary beam energies used. Evidently, neither the silicon, nor the germanium yield dependence on x is fitted by a straight line so that a quantification method based on a ratio of ion yields from an unknown layer to those of a reference material does not extend across the whole of the possible stoichiometry range.

For the purposes of an extended calibration scheme, the measured silicon and germanium ion yields as a function of x were normalized to the silicon ion yield obtained for that particular energy. The 250 and 500 eV silicon ion yields were found to be well fitted by quartics, the 750 eV a cubic, while the 1 keV had a quadratic dependence

$$\text{Si}_{\text{measured}}(250 \text{ eV}) = 1 - 0.02x + 0.5e^{-3}x^2 - 6.6e^{-6}x^3 + 2.6e^{-8}x^4, \tag{6}$$

$$\text{Si}_{\text{measured}}(500 \text{ eV}) = 1 - 0.02x + 5.7e^{-4}x^2 - 9.1e^{-6}x^3 + 4.4e^{-8}x^4, \tag{7}$$

$$\text{Si}_{\text{measured}}(750 \text{ eV}) = 1 - 9.1e^{-3}x - 6.5e^{-5}x^2 + 5.6e^{-7}x^3, \tag{8}$$

$$\text{Si}_{\text{measured}}(1 \text{ keV}) = 1 - 0.01289x + 3.033e^{-5}x^2. \tag{9}$$

For the germanium ion yields, cubics were again found to fit the behavior well for all but the 1 keV data where a quadratic yielded a good fit

$$\text{Ge}_{\text{measured}}(250 \text{ eV}) = 8.8e^{-3}x + 2.9e^{-5}x^2 + 6.3e^{-7}x^3, \tag{10}$$

$$\text{Ge}_{\text{measured}}(500 \text{ eV}) = 0.01x + 1.0e^{-4}x^2 - 5.5e^{-7}x^3, \tag{11}$$

$$\text{Ge}_{\text{measured}}(750 \text{ eV}) = 0.02x - 1.9e^{-4}x^2 + 1.5e^{-6}x^3, \tag{12}$$

$$\text{Ge}_{\text{measured}}(1 \text{ keV}) = 0.02x - 3.4e^{-5}x^2. \tag{13}$$

The fits obtained for the 750 eV and 1 keV germanium data do not include the ion yields for pure germanium because the extreme pitting made the ion yields unstable, and so they only span the range of $0 \leq x \leq 0.74$.

The behavior of the ion yields as a function of x [Figs. 7(a)–7(d)] reveals a rather weak nonlinear dependence. This may be due to the underlying trends in ionization probability, or sputter yield, or both. Below, we investigate the partial sputter yield and ratio of the useful yield to the partial sputter yield (a parameter which is proportional to the ionization probability) for Si and Ge.

E. Comparison of partial ion and sputter yields

The SIMS sputter yield can be obtained from the relationship

$$Y = \frac{v_z N}{J}, \tag{14}$$

where Y is the sputter yield, N is the concentration of target atoms, v_z is the erosion rate, and J is the primary ion flux which is given by

$$J = \frac{I}{eA}, \tag{15}$$

where I is the primary beam current, e is the electronic charge, and A is the area from which the ions are sputtered.

Silicon, SiGe, and germanium have a diamond lattice structure and so the number of target atoms per unit volume is given by

$$Z_T = \frac{8}{a^3}. \tag{16}$$

Here, a is the bulk (i.e., SiGe) lattice parameter. The number of silicon and germanium atoms per cubic meter can be determined by multiplying the total number of atoms (Z_T) present by their known fractions.

The partial sputter yields (i.e., the sputter yields of the constituents that make up the target material normalized to their unit concentration (atom/ion cm^3)) for both silicon and germanium as a function of x were determined for comparison with the ion yields. Figures 8(a)–8(h) show these normalized silicon and germanium sputter yields and ion yields, respectively. The silicon sputter yields were normalized to that for pure silicon while the germanium was normalized to pure germanium in the case of the 250 and 500 eV data, and to that for $x=0.74$ for the data above 750 eV due to the difficulty of obtaining a stable germanium ion yield from the pure germanium samples.

From Figs. 8(a)–8(h), the normalized sputter and measured ion yields for changing x do not show proportionality except in the case of the 250 eV germanium. The excellent agreement between the germanium sputter and ion yield at 250 eV suggests a sputtering dependence only. Further support of this is shown when we investigate the ionization probability of the samples. For all the other data, the lack of proportionality indicates that there is another influence affecting the measured ion yield.

The useful ion yield is given by

$$\tau_M = P_M \eta_M, \tag{17}$$

where P_M and η_M are the ionization probability and the product of the collection transmission and detection efficiencies for a species M, respectively. If the instrumental transmission is kept constant, any variation of the useful ion yield will be due to changing ionization probability. The useful yield can be determined from the partial ion yields and the sputter yield

$$I_M = \tau_M Y C_M I_P, \tag{18}$$

where I_M and C_M are the secondary ion yield and concentration of element M, respectively; Y is the total matrix sputter yield and I_P is the incident ion current.

Figures 9(a) and 9(b) show the silicon and germanium useful yields for the different primary beam energies as a
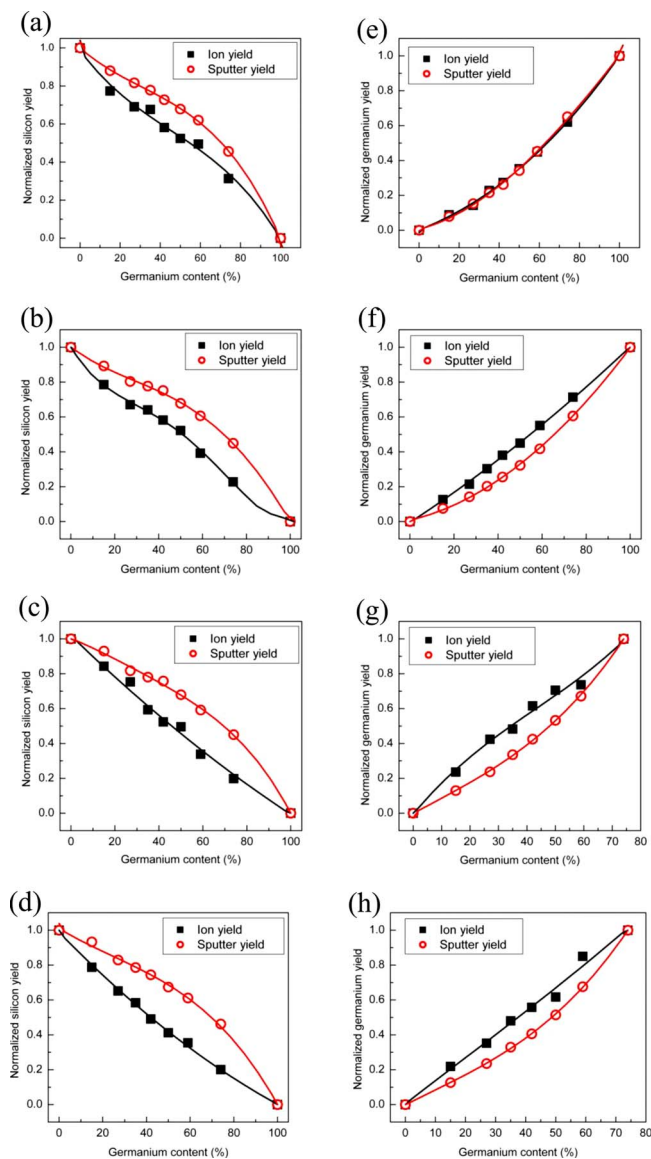

FIG. 8. (Color online) Normalized silicon and germanium ion and sputter yields as a function of germanium content. (a) 250 eV silicon, (b) 500 eV silicon, (c) 750 eV silicon (d) 1 keV silicon, (e) 250 eV germanium, (f) 500 eV germanium, (g) 750 eV germanium, and (h) 1 keV germanium.

function of x. Both show a decrease for increasing x except for the germanium yield at 250 eV which remains almost constant. One possible reason for the drop in useful yields is that there is a reduction in the steady-state concentration of oxygen at the surface because of the increasing erosion rate and increased oxygen backscattering with x.

From the germanium useful yields shown in Fig. 9(b), two features stand out. One is the constant useful ion yield with x at 250 eV, while the other is the significant drop in useful ion yield at 1 keV. The 250 eV germanium ion yield behavior indicates that the ionization probability is independent of x and that a constant oxygen presence is achieved around the germanium atoms within the altered layer region for all x. It can also be noted that from Figs. 9(a) and 9(b), the variation in useful ion yield as a function of x is reduced the lower the beam energy used. This indicates that, in general, the dependence of ionization on x becomes less influential for lower beam energies.
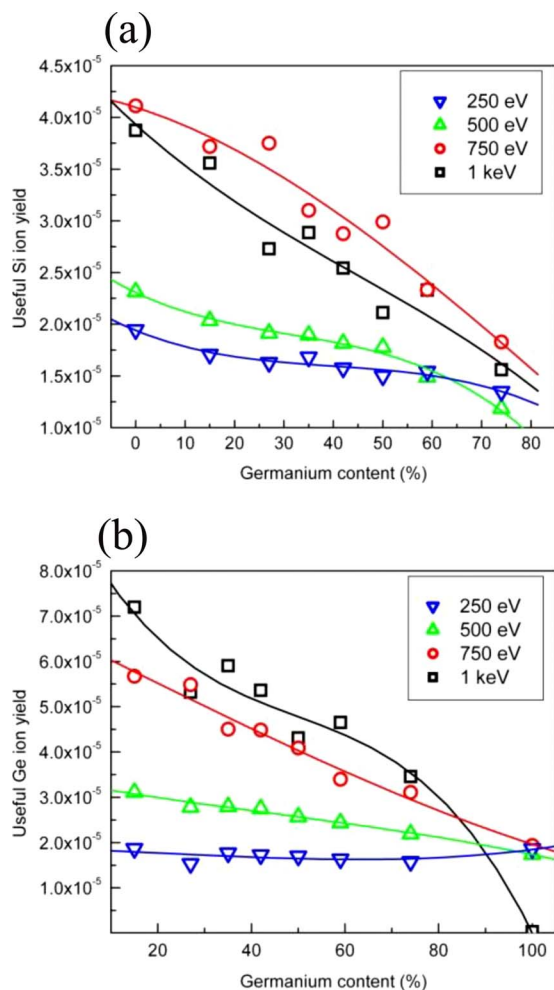
FIG. 9. (Color online) Calculated silicon and germanium useful ion yields as a function of germanium content for primary beam energies 250 eV, 500 eV, 750 eV, and 1 keV. (a) Silicon useful yield and (b) germanium useful yield.

The large drop in useful germanium yield for 1 keV shows a low ionization probability, and is in good agreement with previous work which found that a 3 keV oxygen beam failed to oxidize germanium.[20] The relationship between germanium ion yield and beam energy observed here implies that germanium is more aggressively oxidized below an energy threshold somewhere between 750 eV and 1 keV. Increased oxygen incorporation would also explain the improved uniformity achieved for germanium sputtering at lower energies (i.e., ≤ 500 eV) and the large jump in erosion rate between 750 eV and 1 keV. The formation of a fully oxidized altered layer in silicon is directly associated with significantly reduced erosion rates and (at near normal incidence) planarization during erosion.

IV. CONCLUSIONS

This work gives a basis for the quantification of x in $Si_{1-x}Ge_x$ for the range of $0 \leq x \leq 1$ over the variety of beam energies commonly referred to as "ultralow energy" and for O_2^+ bombardment at normal incidence. We show that the erosion rates have an exponentially increasing dependence on increasing x. When the SiGe erosion rates for different

energies are normalized to that of silicon, their variation with x becomes almost identical. This has the potential (for certain samples) of enabling the stoichiometry of a $Si_{1-x}Ge_x$ layer to be quantified (or the quantification checked) from the relative erosion rate.

Silicon and germanium ion yields as a function of x do not exhibit affine behavior over the whole range and the apparent proportional behavior for Ge in layers in the range of $x \leq 30\%$ is just a consequence of the restricted range. Yields are (pragmatically) well fitted by polynomials with degrees between 2 and 4 from which accurate quantification of the matrix should be possible. For energies ≥ 750 eV the measured ion yields for pure germanium showed either instability or a loss of intensity with depth compared to lower beam energies (≤ 500 eV). Optical and SEM imaging of the craters revealed large scale topography effects in the form of pitting which is almost certainly linked to the ion yield behavior, perhaps through uneven oxidation of the surface combined with defect nucleation during bombardment. For energies ≤ 500 eV atomically flat high depth resolution quality crater bottoms are formed with a transition to less advantageous behavior between 500 and 750 eV. Therefore, only for energies ≤ 500 eV can good profiling topography and ion yield behavior be routinely achieved for pure germanium layers.

In measurements of useful ion yields for different beam energies as a function of x, the 250 eV germanium ion yield is found to be proportional to its sputter yield. Furthermore, the useful germanium yield at this energy remained constant (to within 10%) with x—there is no significant matrix effect.

A significant drop in the useful yield for germanium at 1 keV indicated that germanium was not efficiently oxidized at this energy. For beam energies ≤ 750 eV the magnitude of the useful yield for germanium was similar to that in the SiGe layers suggesting that germanium oxidizes more readily under these conditions. It is likely that the onset of efficient ionization is linked to improved sputtering topography and the closer similarity between erosion rates observed for germanium at lower (e.g., ≤ 500 eV) primary beam energies. The underlying cause would be improved oxygen incorporation and a fully oxidized altered layer. Further work using high-resolution transmission electron microscopy and electron-energy-loss spectroscopy will help to verify this conclusion.

Previous findings have shown SIMS capable of determining the $Si_{1-x}Ge_x$ ($x \leq 0.3$) matrix composition to within ± 1 at. %,[7] while the results here indicate a similar level of accuracy should be achievable for the extended range of ($0 < x < 1$) and using reference materials. This level of accuracy is certainly comparable with alternative analytical techniques such as energy dispersive x ray and Auger electron spectroscopy (± 2 at. %),[21,22] while high resolution Rutherford backscattering and HRXRD offer ± 1 at. %.[6,7]

[1]E. Kasper and S. Heim, Appl. Surf. Sci. **224**, 3 (2004).

[2]M. J. Lee, E. A. Fitzgrald, M. T. Bulsara, M. T. Currie, and A. Lochtefeld, J. Appl. Phys. **97**, 011101 (2005).

[3]T. E. Whall and E. H. C. Parker, Thin Solid Films **367**, 250 (2000).

[4]E. Kasper, Appl. Surf. Sci. **254**, 6158 (2008).

[5]G. Dong, C. Liangzhen, L. Rong, and A. T. S. Wee, Surf. Interface Anal. **32**, 171 (2001).

[6]F. Sánchez-Almazán, E. Napolitani, A. Carnera, A. V. Drigo, M. Berti, J. Stangl, Z. Zhong, G. Bauer, G. Isella, and H. von Känel, Nucl. Instrum. Methods Phys. Res. B **226**, 301 (2004).

[7]M. G. Dowsett, R. Morris, P.-F. Chou, S. F. Corcoran, S. Kheyrandish, G. A. Cooke, J. L. Maul, and S. B. Patel, Appl. Surf. Sci. **203-204**, 500 (2003).

[8]A. Mikami, T. Okazawa, K. Saito, and Y. Kido, Appl. Surf. Sci. **253**, 1620 (2006).

[9]M. Kummer, C. Rosenblad, A. Dommann, T. Hackbarth, G. Höck, M. Zeuner, E. Müller, and H. von Känel, Mater. Sci. Eng., B **89**, 288 (2002).

[10]J. W. Matthews and A. E. Blakeslee, J. Cryst. Growth **27**, 118 (1974).

[11]P. J. Wang, M. S. Goorsky, B. S. Meyerson, F. K. LeGoues, and M. J. Tejwani, Appl. Phys. Lett. **59**, 814 (1991).

[12]D. K. Bowen and B. K. Tanner, *High Resolution X-Ray Diffraction and Topography* (Taylor & Francis, London, 1998).

[13]P. F. Fewster, Semicond. Sci. Technol. **8**, 1915 (1993).

[14]W. De Coster, B. Brijs, and W. Vandervorst, in *Proceedings of Secondary Ion Mass Spectrometry X*, edited by A. Bennighoven, B. Hagenhoff, and H. W. Werner (Wiley, New York, 1997), p. 529.

[15]H. Xing, D. S. Green, H. Yu, T. Mates, P. Kozodoy, S. Keller, S. P. Denbaars, and U. K. Mishra, Jpn. J. Appl. Phys., Part 1 **42**, 50 (2003).

[16]P. C. Zalm, C. J. Vriezema, D. J. Gravesteijn, G. F. A. van der Walle, and W. B. de Boer, Surf. Interface Anal. **17**, 556 (1991).

[17]M. G. Dowsett, T. J. Ormsby, F. S. Gard, S. H. Al-Harthi, B. Guzmán, C. F. McConville, T. C. Q. Noakes, and P. Bailey, Appl. Surf. Sci. **203-204**, 363 (2003).

[18]M. G. Dowsett and E. A. Clark, *Practical Surface Analysis*, 2nd ed., edited by D. Briggs and M. P. Sears (Wiley, New York, 1992), Chap. 5, p. 229.

[19]Z. X. Jiang, K. Kim, J. Lerma, A. Corbett, D. Sieloff, M. Kottke, R. Gregory, and S. Schauer, Appl. Surf. Sci. **252**, 7262 (2006).

[20]C. Huyghebaert, T. Conard, B. Brijs, and W. Vandervorst, Appl. Surf. Sci. **231-232**, 708 (2004).

[21]R. Loo, H. Sorada, A. Inoue, B. C. Lee, S. Hyun, S. Jackschik, G. Lujan, T. Y. Hoffmann, and M. Caymax, Semicond. Sci. Technol. **22**, S110 (2007).

[22]D. Krüger, A. Penkov, Y. Yamamoto, A. Goryachko, and B. Tillack, Appl. Surf. Sci. **224**, 51 (2004).